[Paleoceanography]

Supporting Information for

[Coherent response of Antarctic Intermediate Water and Atlantic Meridional Overturning Circulation during the last deglaciation: reconciling contrasting neodymium isotope reconstructions in tropical Atlantic]

Sifan Gu[a,*], Zhengyu Liu[a,b,*], Jiaxu Zhang[a], Johannes Rempfer[c], Fortunat Joos[c], Esther C. Brady[d], Delia W. Oppo[e]

[a]Department of Atmospheric and Oceanic Sciences and Center for Climatic Research, University of Wisconsin-Madison, Madison, WI, USA;

[b]Laboratory Climate, Ocean and Atmosphere Studies, Peking University, Beijing, China;

[c]Climate and Environmental Physics, Physics Institute and Oeschger Center for Climate Change Research, University of Bern, Bern, Switzerland

[d]Climate and Global Dynamics Division, National Center for Atmospheric Research, Boulder, CO, USA

[e]Department of Geology and Geophysics, Woods Hole Oceanographic Institution, Woods Hole, MA, USA

Contents of this file

Introduction

We show additional figures about Nd module validation under present day climate forcing. We also show the results in an idealized hosing experiment and confirm that the relationship between AAIW and AMOC in iPOP-TRACE is robust. In addition, we discuss potential influence of changes in the relative contributions from west and east North Atlantic Deep Water.

Text S1. AAIW evolution in idealized hosing experiment

We performed an idealized freshwater hosing experiment following *Rempfer et al.*, [2012] to further examine the relationship between AAIW and AMOC. The results are consistent with the transient run (iPOP2-TRACE). This experiment was initiated from CTRL and was carried out under the same forcing as CTRL, except that with periodic fresh water perturbation applied over North Atlantic between 45°N and 70°N. The maximum amplitude of freshwater fluxes is 0.3Sv and the period is 2000 years. Freshwater fluxes vary linearly between 0.3Sv and -0.3Sv (Fig. S4B black). The rate of freshwater increase is small so that the system is close to equilibrium. We run this experiment for 5000 years and show a composite of two periods from 1000 to 5000 model year.

AAIW northward penetration covaries with AMOC strength in this freshwater hosing experiment as in iPOP2-TRACE. AMOC strength varies with the changing fresh water forcing (Fig. S4B navy). AMOC strength reaches its maximum at year 500. Its strength is 25 Sv and NADW fills most of the Atlantic basin (Fig. S5A). AMOC reaches its minimum at year 1550 after freshwater input. Overturning circulation is sluggish and NADW formation is largely weakened (Fig. S4B). AAIW ε_{Nd} end-member value is nearly stable around -8.0 during the whole experiment (Fig. S4D dashed brown), therefore AAIW ε_{Nd} at equatorial Atlantic indicates a stronger AAIW northward penetration when AMOC is strong (Fig. S4D solid brown). When AMOC is weak, AAIW is confined in South Atlantic (Fig. S5D) because of reduced AAIW northward transport (Fig. S5F), just as the HS1 in iPOP2-TRACE. AAIW is also deeper when AMOC is weaker (Figs. S4C, S5C and S5D). Winter surface density in NADW and AAIW formation regions also reverses between AMOC maximum and AMOC minimum case (Fig.S4A). During AMOC maximu, σ_{NADW} (27.45 kg/m^3) > σ_{AAIW} (26.7 kg/m^3). During AMOC minimu, σ_{AAIW} (27.9 kg/m^3) > σ_{NADW} (26.2 kg/m^3). However, there is still no counterclockwise

AAIW cell in the overturning streamfunction in AMOC minimum case (Fig. S5B). Therefore, the conclusions we drawn from iPOP2-TRACE are robust.

Text S2. Potential influence of the changes in west and east NADW

In our simulation, the influence of potential changes in the relative contribution from NW versus NE Atlantic deep waters is negligible. Firstly, the influence of NADW is around 1200m – 2600m (Fig. 5A). In this study, we are focusing on the intermediate water, which is above deep water range. Secondly, we show the ε_{Nd} evolutions at four different locations in the North Atlantic in Fig. S8. Fig. S8 A and B show the evolution in the deep water formation region in the west and east North Atlantic respectively. During HS1, ε_{Nd} in the west becomes more radiogenic (Fig. S8A) with a ε_{Nd} change of ~1.5, while the ε_{Nd} change from 2,000m to 3,000m in the east show ε_{Nd} change of ~0.25. However, ε_{Nd} evolution away from NADW formation region (Fig. S8 C and D), ε_{Nd} at around 2,000m shows very small changes, ~0.25. Therefore, changes in the relative contribution from NW versus NE North Atlantic deep water formation does not have much influence on the NADW ε_{Nd} value in our simulation away from the NADW formation region. This is consistent with the findings in Rempfer et al., [2012], which suggest that the endmember ε_{Nd} change is rather small compared with ε_{Nd} changes due to changes in watermass distribution. In addition, in the upper several hundred meters, all sites show a less radiogenic change from the LGM to the HS1, which is because of the reduced influence of water from Caribbean Sea and Gulf of Mexico as discussed in section 4.

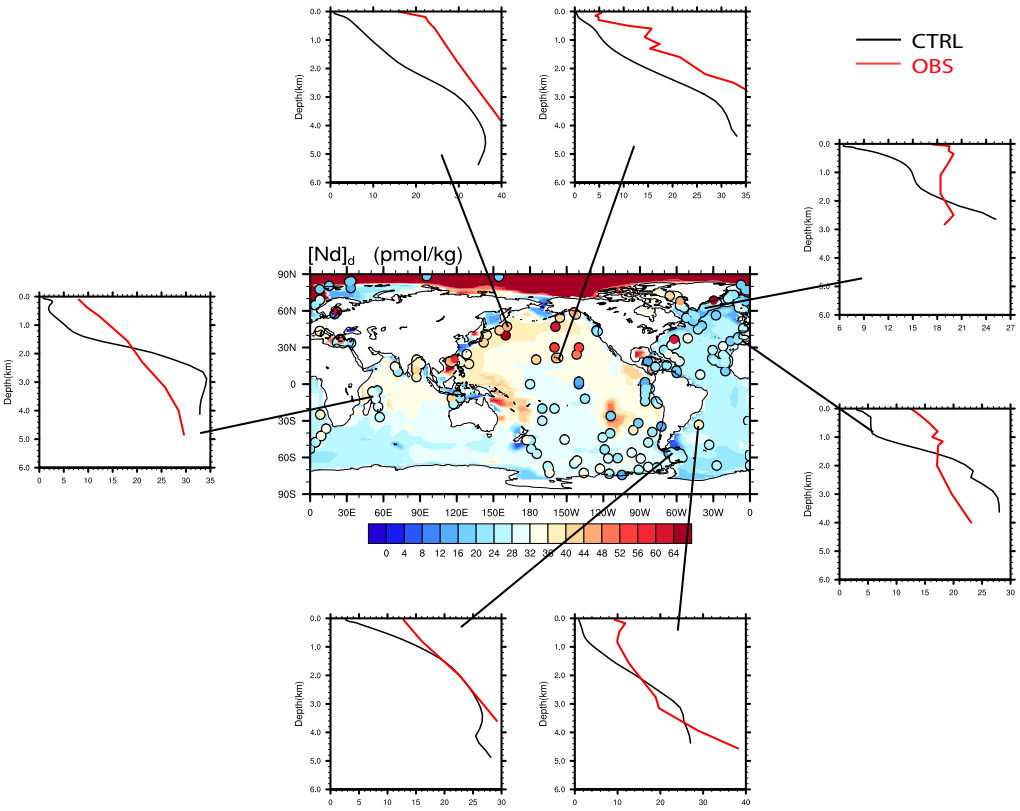

Figure S1. Comparison of Nd concentration fields between model and observation. Global map of Nd concentration at the sea floor from the equilibrium state in CTRL. Observations [*van de Flierdt et al.*, 2016] are superimposed as filled circles, using the same color scale. Selected vertical profiles show observed (red) and simulated (black) Nd concentration.

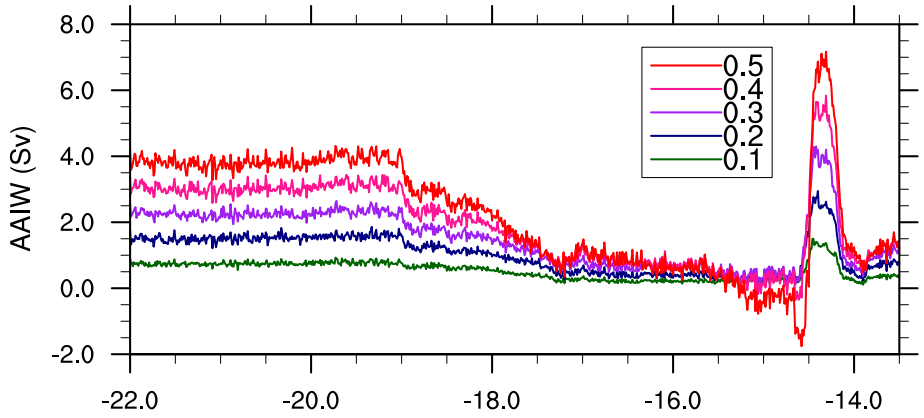

Figure S2. Northward transport at equatorial Atlantic of layers between (σ_{AAIW} -n) and (σ_{AAIW} +n): n = 0.5 (red), 0.4 (magenta), 0.3 (purple), 0.2 (navy) and 0.1 (green).

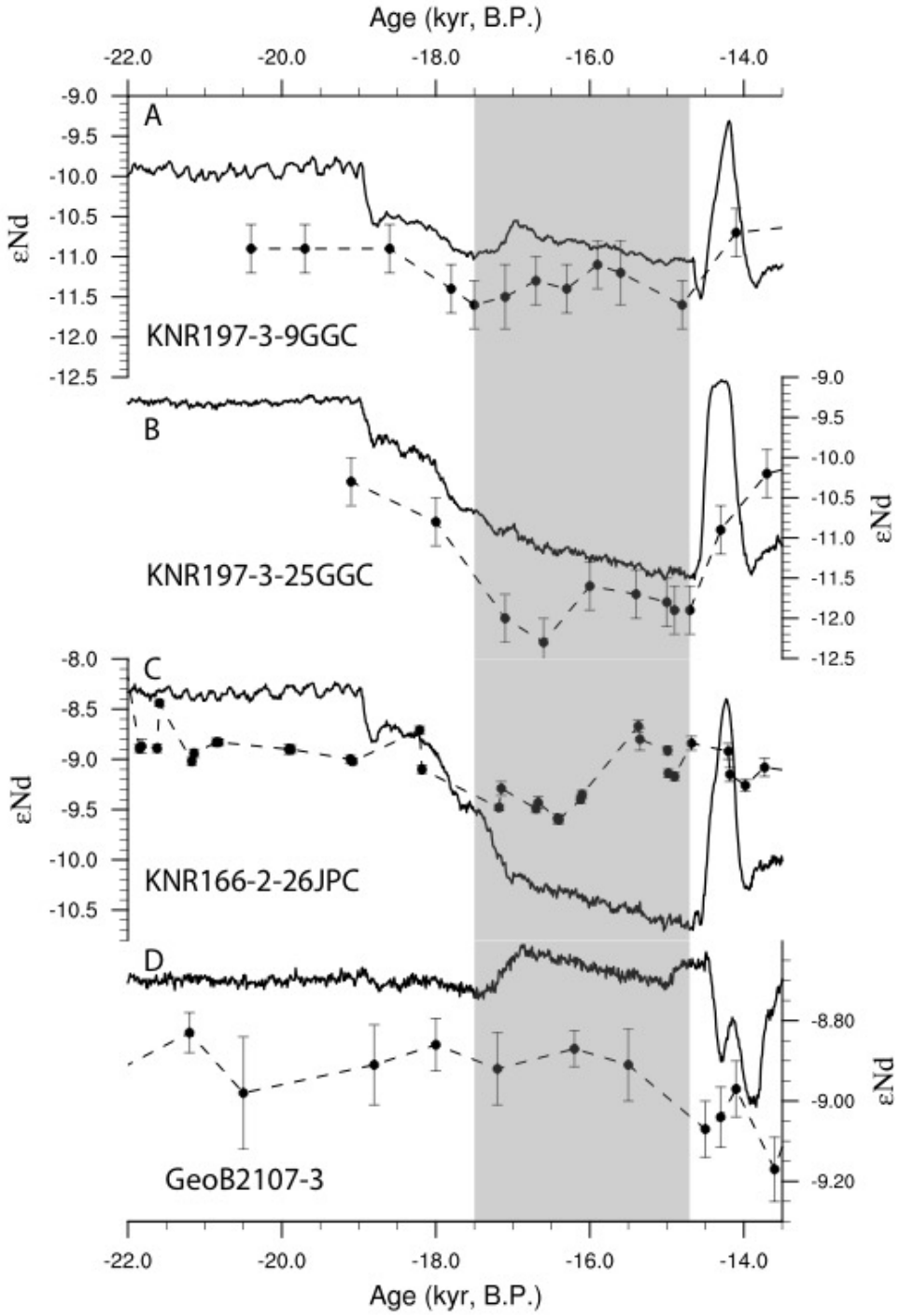

Figure S3. Comparison between model ε_{Nd} (solid) with reconstructions (dash). (A) KNR197-3-9GGC in Demerara Rise (7°55.8'N, 53°34.51'W, 1100m) [*Huang et al.*, 2014]. (B) KNR197-3-25GGC in Demerara Rise (7°42.27'N, 53°47.12'W, 671m) [*Huang et al.*, 2014]. (C) KNR166-2-26JPC in the Florida Straits (24°19.62'N, 83°15.14'W, 546m) [*Xie et al.*, 2012]. (D) GeoB2107-3 in southern Brazil margin (27.2°S, 46.5°W, 1050m) [*Howe et al.*, 2016].

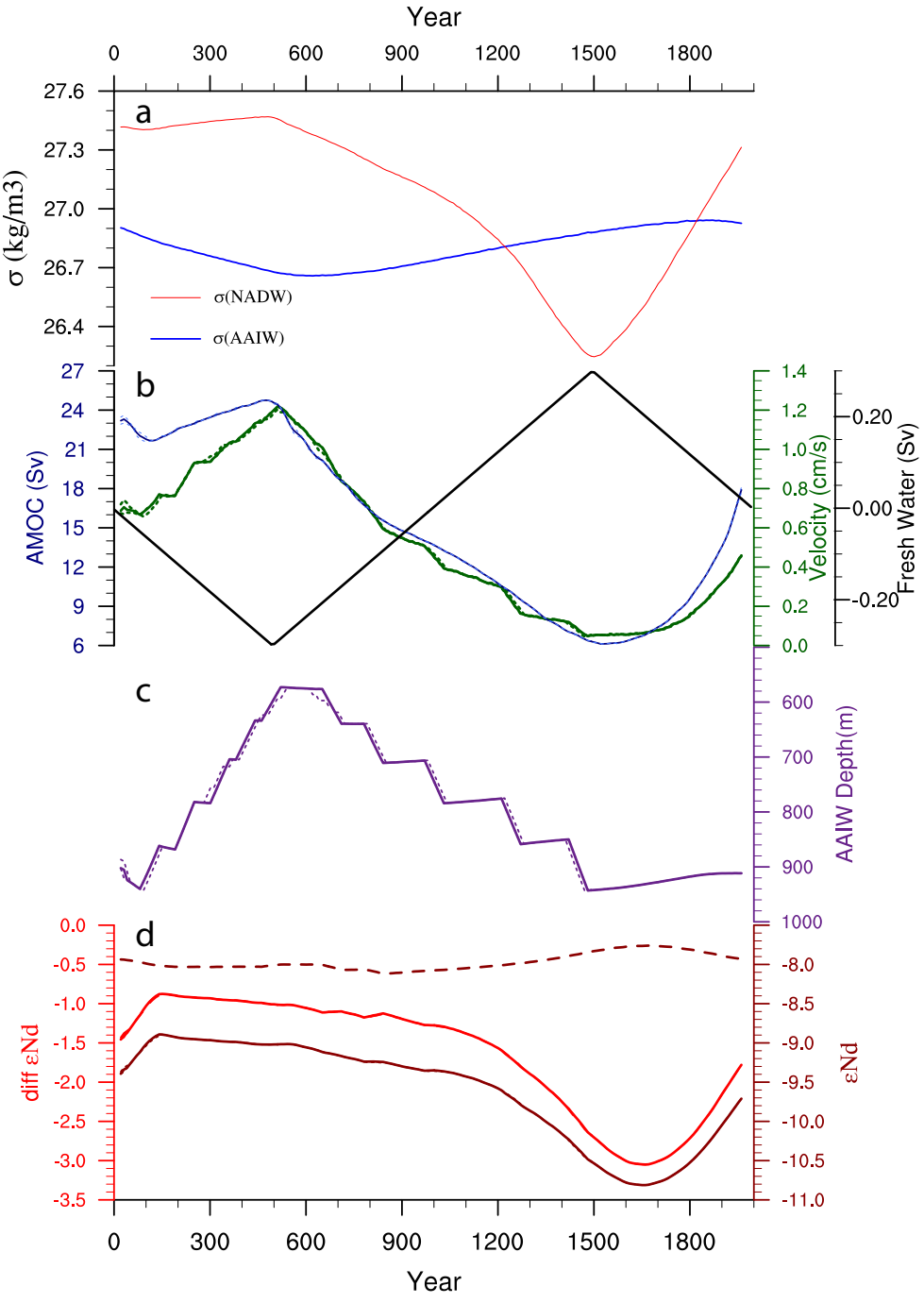

Figure S4. Evolutions in the idealized freshwater discharging experiment. Solid lines for composite and dashed lines for different members. (A) Winter surface density in NADW (red) and AAIW (blue) production region. (B) Periodic freshwater fluxes applied over 45°N to 70°N North Atlantic (black), AMOC response (blue) and meridional velocity (cm/s) at equator σ_{AAIW} (green). (C) AAIW depth. (D)

AAIW endmember ε_{Nd} value (dashed brown), zonal mean AAIW ε_{Nd} value at equator (solid brown) and the difference between AAIW ε_{Nd} value at equator and AAIW endmember ε_{Nd} value (red).

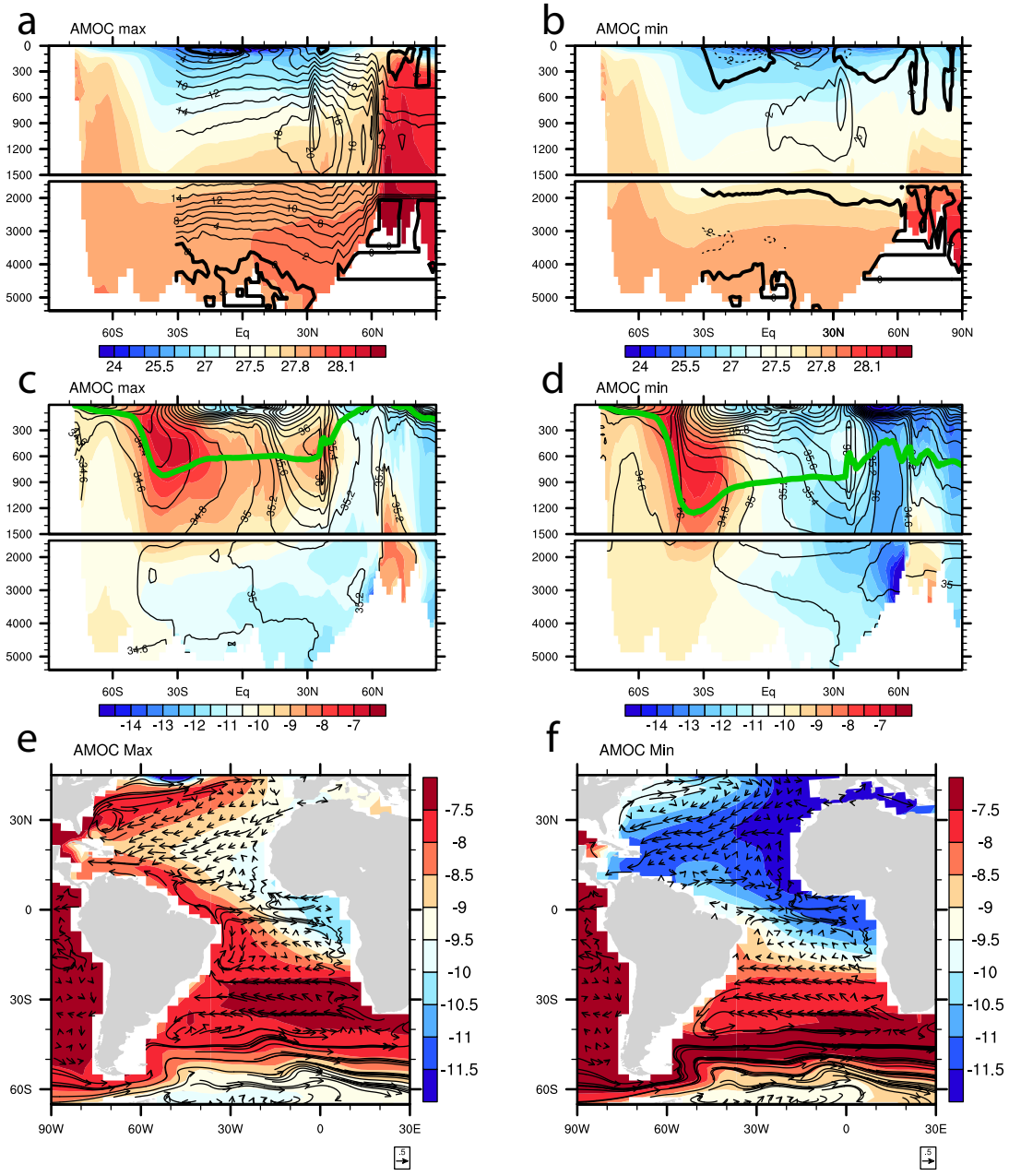

Figure S5. Comparison between AMOC maximum and AMOC minimum in idealized hosing experiment. Atlantic meridional overturning streamfunction (line) and Atlantic zonal mean potential density (color) during AMOC maximum (A), and AMOC minimum (B). Atlantic zonal mean ε_{Nd} (colored), salinity (black contour) and isopycnal line for σ_{AAIW} (green line): (C) AMOC maximum and (D) AMOC

minimum. ε_{Nd} at σ_{AAIW} surface (color) with velocity fields (cm/s) superimposed as vectors: (E) AMOC maximum at density surface of 27.29 kg/m^3; (F) AMOC minimum at density surface of 27.38 kg/m^3.

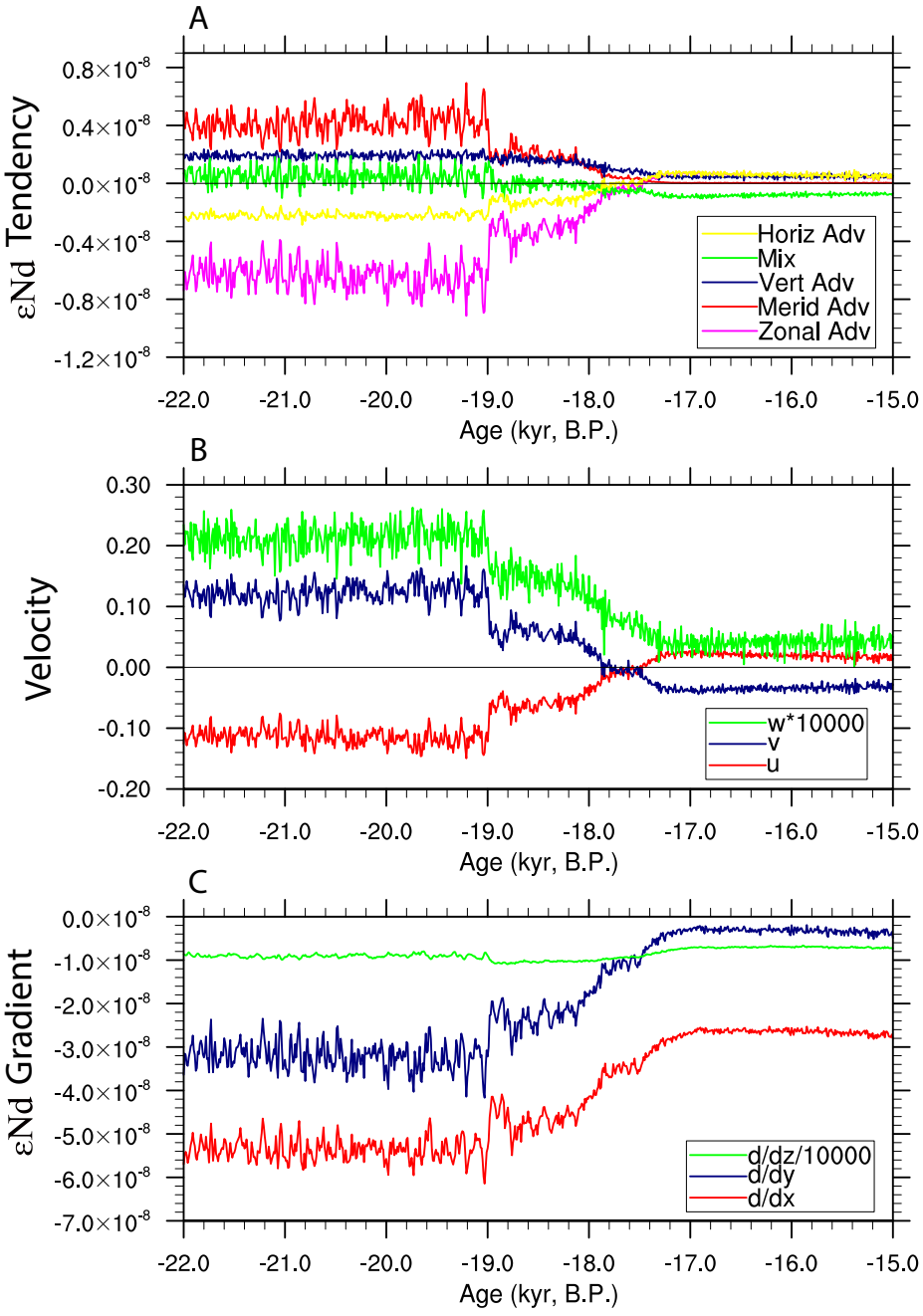

Figure S6. ε_{Nd} tracer budget analysis for (12°N, 75°W, 1330m), which is near MD99-2198. A, time series of ε_{Nd} tendency terms: zonal advection (magenta), meridional advection (red), horizontal advection (zonal advection + meridional advection) (yellow), vertical advection (navy) and mixing (green). B, evolution of velocity: zonal velocity (u) (red), meridional velocity (v) (navy) and vertical velocity multiplied by 10^4 (w) (green). C, ε_{Nd} gradient: zonal gradient (red), meridional gradient (navy) and vertical gradient (green).

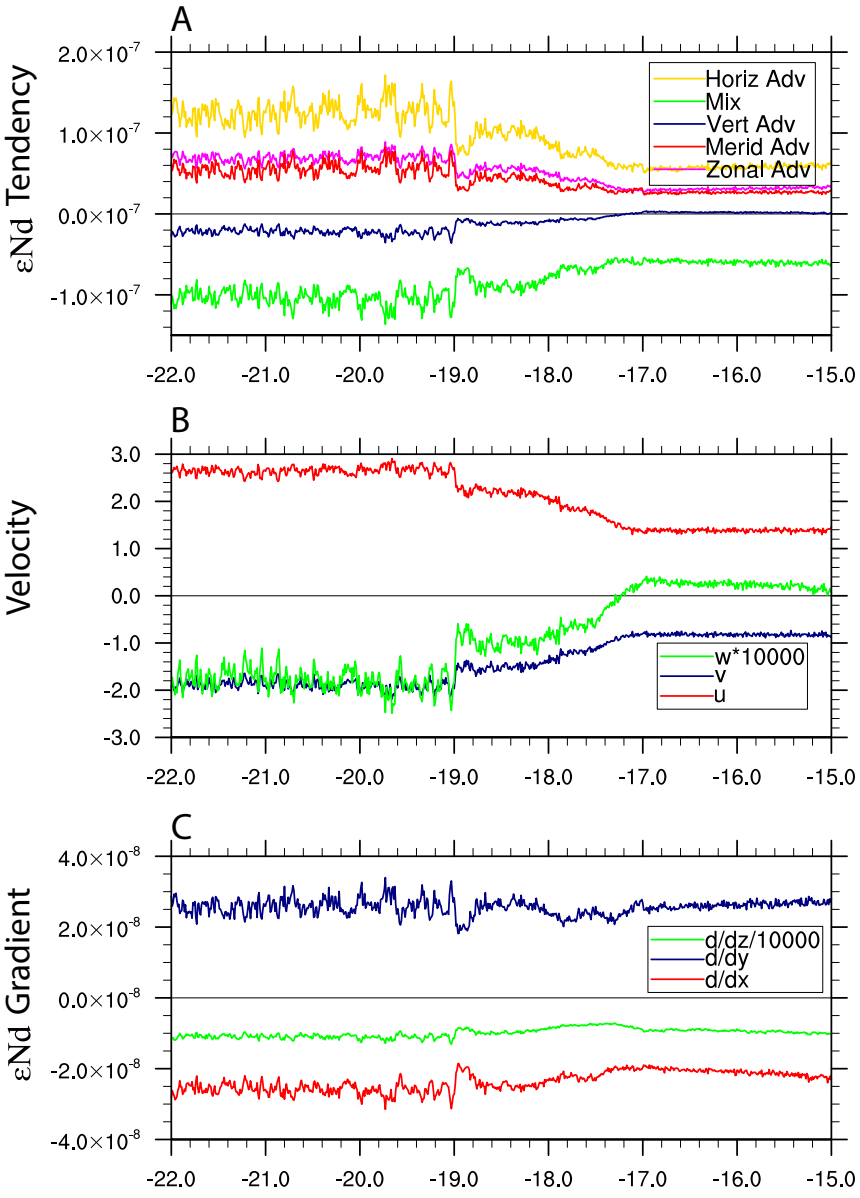

Figure S7. ε_{Nd} tracer budget analysis for site KNR166-2-26JPC. A, time series of ε_{Nd} tendency terms: zonal advection (magenta), meridional advection (red), horizontal advection (zonal advection + meridional advection) (yellow), vertical advection (navy) and mixing (green). B, evolution of velocity: zonal velocity (u) (red), meridional velocity (v) (navy) and vertical velocity multiplied by 10^4 (w) (green). C, ε_{Nd} gradient: zonal gradient (red), meridional gradient (navy) and vertical gradient (green).

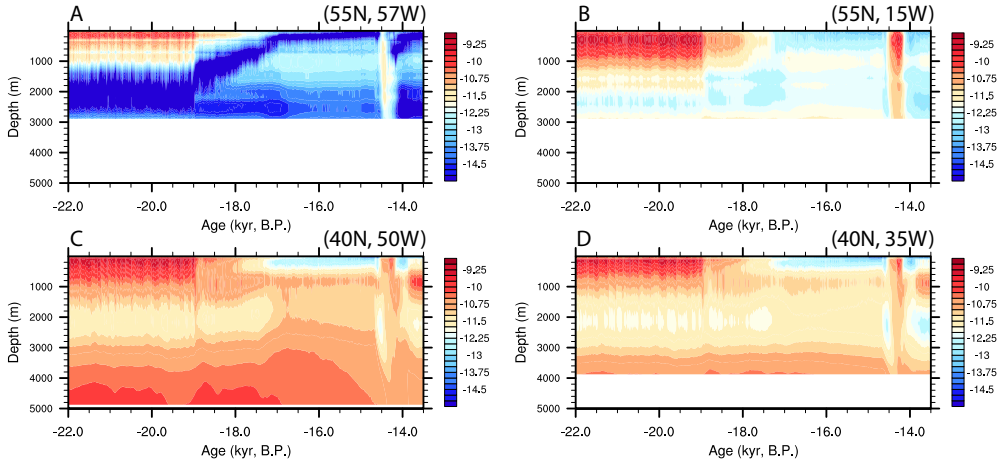

Figure S8: ε_{Nd} evolution at four North Atlantic sites. (A) (55°N, 57°W), which is near Labrador Sea Water formation region; (B) (55°N, 15°W), which is in the east Atlantic; (C) (40°N, 50°W), which is in the west boundary; (D) (45°N, 35°W), which is in the center of Atlantic.

Reference:

van de Flierdt, T., A. M. Griffiths, M. Lambelet, S. H. Little, T. Stichel, and D. J. Wilson (2016), Neodymium in the oceans: a global database, a regional comparison and implications for palaeoceanographic research, *Philos. Trans. R. Soc. A Math. Phys. Eng. Sci.*, *374*(2081), 20150293, doi:10.1098/rsta.2015.0293.

Howe, J. N. W., A. M. Piotrowski, D. W. Oppo, K.-F. Huang, S. Mulitza, C. M. Chiessi, and J. Blusztajn (2016), Antarctic Intermediate Water circulation in the South Atlantic over the past 25,000 years, *Paleoceanography*, doi:10.1002/2016PA002975.

Huang, K.-F., D. W. Oppo, and W. B. Curry (2014), Decreased influence of Antarctic intermediate water in the tropical Atlantic during North Atlantic cold events, *Earth Planet. Sci. Lett.*, *389*, 200–208, doi:10.1016/j.epsl.2013.12.037.

Rempfer, J., T. F. Stocker, F. Joos, and J.-C. Dutay (2012), On the relationship between Nd isotopic composition and ocean overturning circulation in idealized freshwater discharge events, *Paleoceanography*, *27*(3), doi:10.1029/2012PA002312.

Xie, R. C., F. Marcantonio, and M. W. Schmidt (2012), Deglacial variability of Antarctic Intermediate Water penetration into the North Atlantic from authigenic neodymium isotope ratios, *Paleoceanography*, *27*(3), doi:10.1029/2012PA002337.